

iScience, Volume 25

Supplemental information

Obesity modulates cell-cell interactions during ovarian folliculogenesis

Xin Long, Qiuyun Yang, Jingjing Qian, Huiying Yao, Rui Yan, Xin Cheng, Qiancheng Zhang, Chan Gu, Fei Gao, Hongmei Wang, Lin Zhang, and Fan Guo

Figure S1

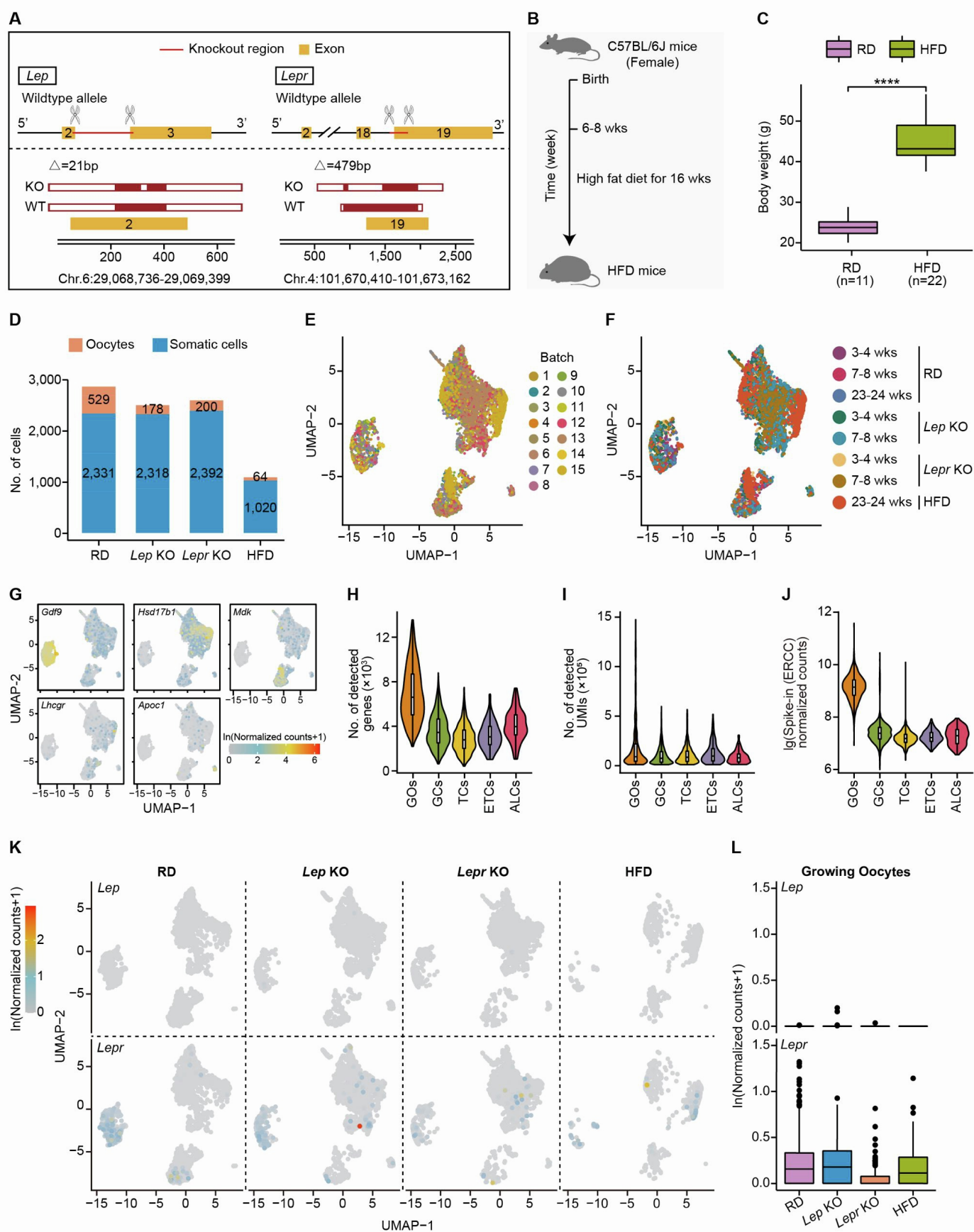


Figure S1. Quality control data for this study. Related to Figure 1

A, CRISPR/Cas9 knockout strategy for constructing *Lep* KO and *Lepr* KO mouse model.

B, Schematic diagram of generating HFD mice.

C, Box plot showing a significant difference in the body weight between RD and HFD mice used in this study (unpaired two-tailed t-test). RD, regular diet; HFD, high-fat diet. ****P ≤ 0.0001 (unpaired two-tailed t-test)

D, Stacked bar plot showing the number of sequenced single cells in RD, *Lep* KO, *Lepr* KO, and HFD mice, grouped by oocytes and somatic cells.

E-F, UMAP (Uniform Manifold Approximation and Projection) embedding visualization for 6,471 single cells from mouse ovarian follicles. Cells are color coded by sequencing batches (E) and the age of mice (F).

G, UMAP embedding visualization of cells in Figure 1B. Cells are color coded by expression levels of *Gdf9*, *Hsd17b1*, *Mdk*, *Lhcgr* and *Apoc1*, respectively.

H-J, Violin plot showing the number of detected genes (H), UMIs (I), and log-transformed ERCC spikes-in normalized counts (J) in an individual cell.

K, UMAP embedding visualization of cells in Figure 1B. Cells are color coded by expression levels of *Lep* or *Lepr*.

L, Box plots showing expression levels of *Lep* (top) and *Lepr* (bottom) in growing oocytes from RD, *Lep* KO, *Lepr* KO and HFD mice.

Figure S2

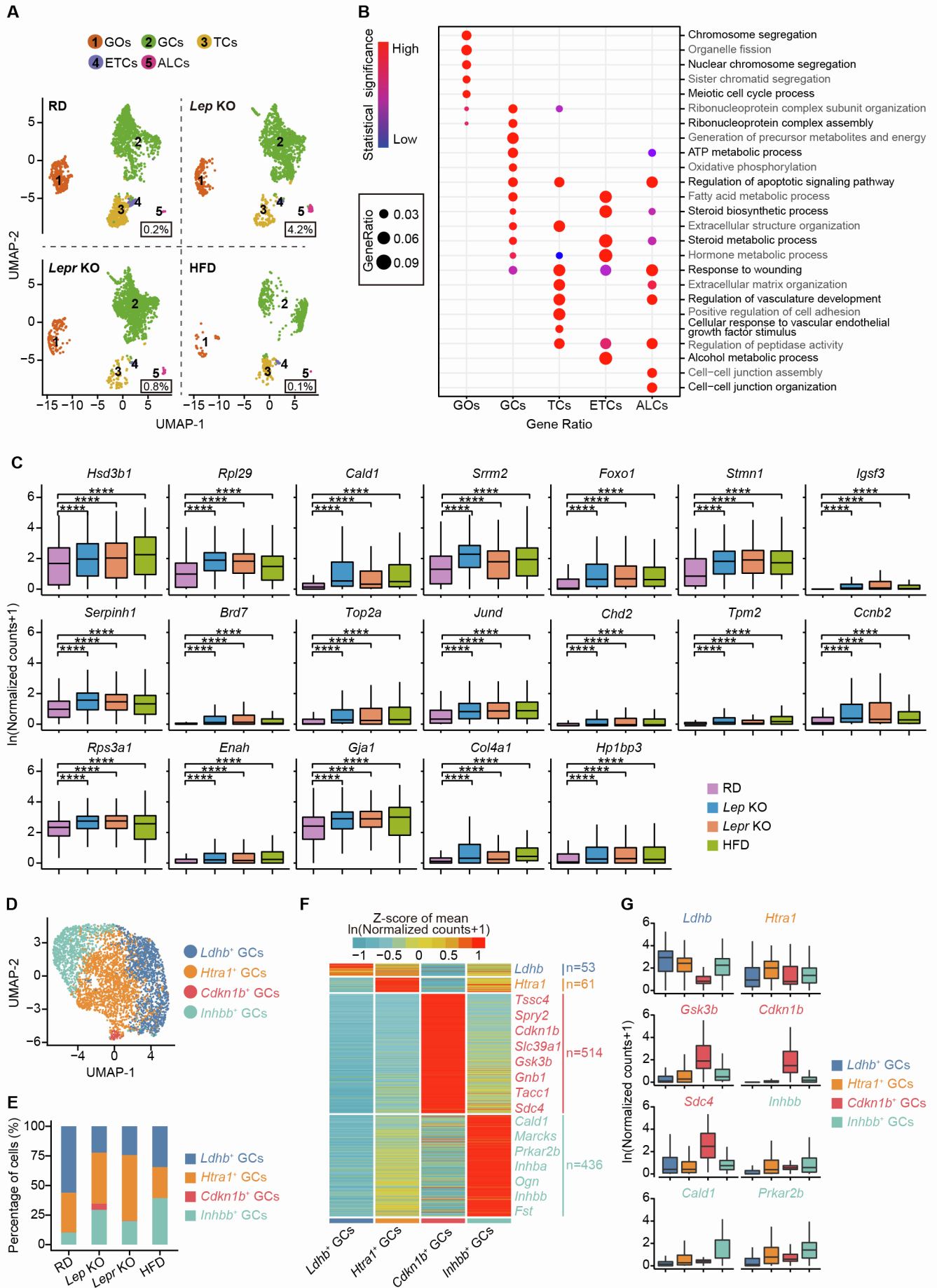


Figure S2. Cell subpopulations identified in granulosa cells from RD and obese mice. [Related to Figure 2](#)

A, UMAP embedding visualization of cells in Figure 1B in RD, *Lep* KO, *Lepr* KO and HFD mice, respectively. Cells are color coded by populations identified. The percentage of ALCs in each mouse models was shown.

B, Gene Ontology (GO) enrichment analysis for five major cell populations identified in Figure 1B. Those differentially expressed genes (DEGs) among cell populations were investigated for enrichment analysis (overrepresentation test).

C, Box plots showing expression levels of commonly up-regulated genes in GCs from the obese mice. ****P ≤ 0.0001 (Wilcoxon rank sum test).

D, UMAP embedding visualization of four subpopulations in granulosa cells identified in Figure 1B. Cells are color coded by subpopulations identified.

E, Stacked bar plot showing the percentage of subpopulations of granulosa cells in RD and obese mice, respectively.

F, Heat map depicting DEGs among all identified subpopulations. Gene expression levels were averaged and scaled.

G, Box plots showing expression levels of representative genes in subpopulations identified.

Figure S3

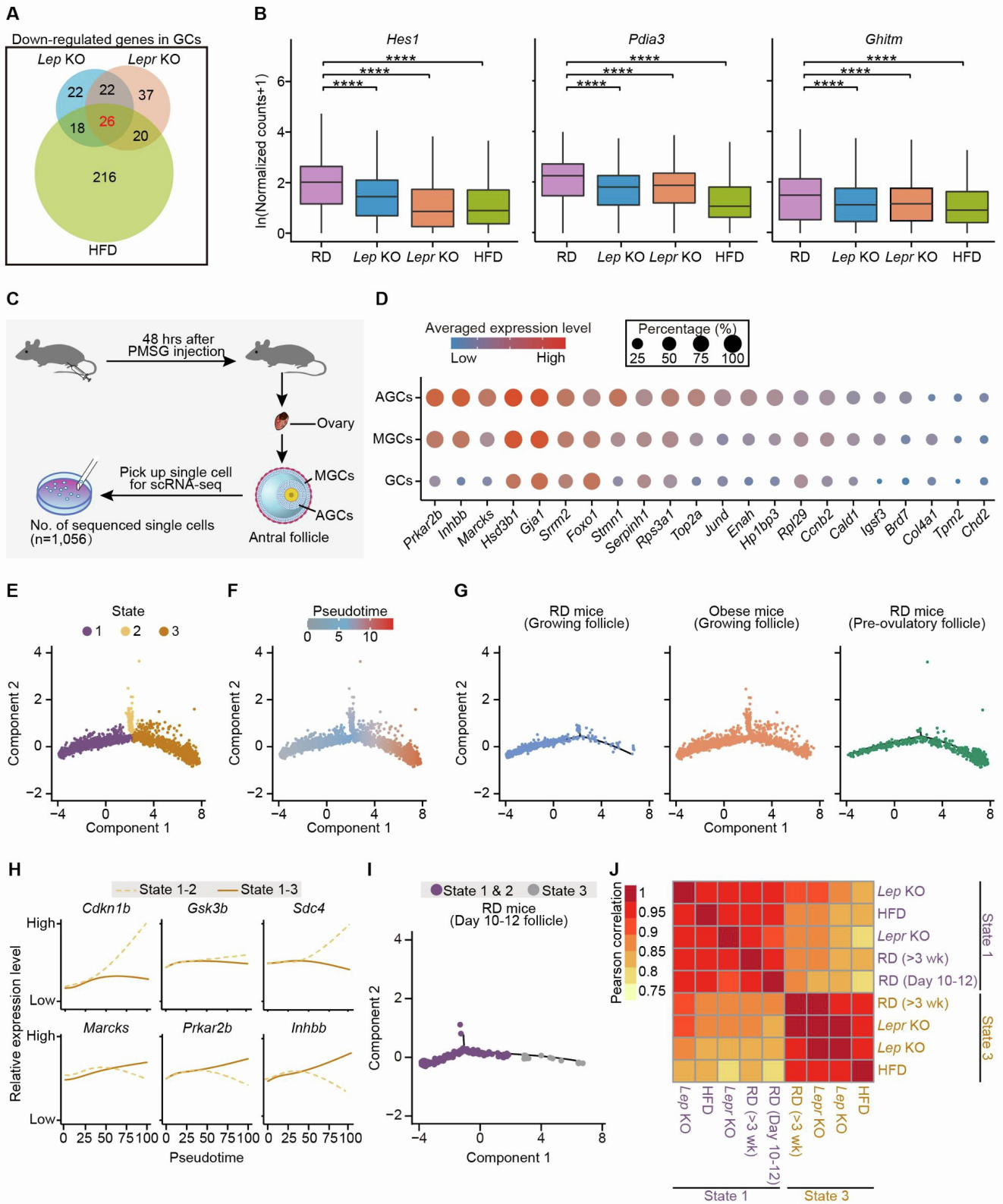


Figure S3. Genes expression in obese GCs and pseudotime analysis for single cell trajectory.

Related to Figure 2

A, Venn diagram showing the down-regulated genes in GCs overlapping among *Lep* KO, *Lepr* KO and HFD mice compared with RD mice.

B, Box plots showing expression levels of *Hes1*, *Pdia3* and *Ghitm* in GCs from RD, *Lep* KO, *Lepr* KO and HFD mice, respectively. The asterisks above indicate statistical significance. ****P <= 0.0001 (Wilcoxon rank sum test).

C, Schematic representation of single-cell RNA-seq of the antral follicles. The number of sequenced single cells is 1,056. AGCs, antral granulosa cells; MGCs, mural granulosa cells.

D, Dot plot depicting the average expression levels of 22 commonly up-regulated genes identified in GCs from the obese mice, in AGCs, MGCs, and GCs from RD mice, respectively. Average expression levels were derived from natural logarithm-scaled normalized counts based on the single-cell RNA-seq data. The percentage of cells expressing the respective gene is indicated by the size of the dot, and only cells with an expression level of greater than 1 for the indicated gene were counted.

E-F, Pseudotime trajectory of granulosa cells in Figure 1B and somatic cells in Pre-ovulatory follicles from RD mice. Trajectory was inferred by Monocle 2. Cells are color coded by State (E) and Pseudotime (F) inferred in the pseudotime analysis, respectively.

G, Pseudotime trajectory of granulosa cells in RD and obese mice. Cells are color coded as indicated.

H, Trend lines showing relative expression levels for representative genes in two branches, State 1-2 and State 1-3, identified by using Monocle2.

I, Pseudotime trajectory of granulosa cells isolated from postnatal day 10-12 mice. Cells are color coded by State identified in the pseudotime analysis.

J, Heat map showing the correlation among GCs in different state from RD and the obese mice as indicated. The Pearson correlation are calculated based on the single-cell RNA-seq data.

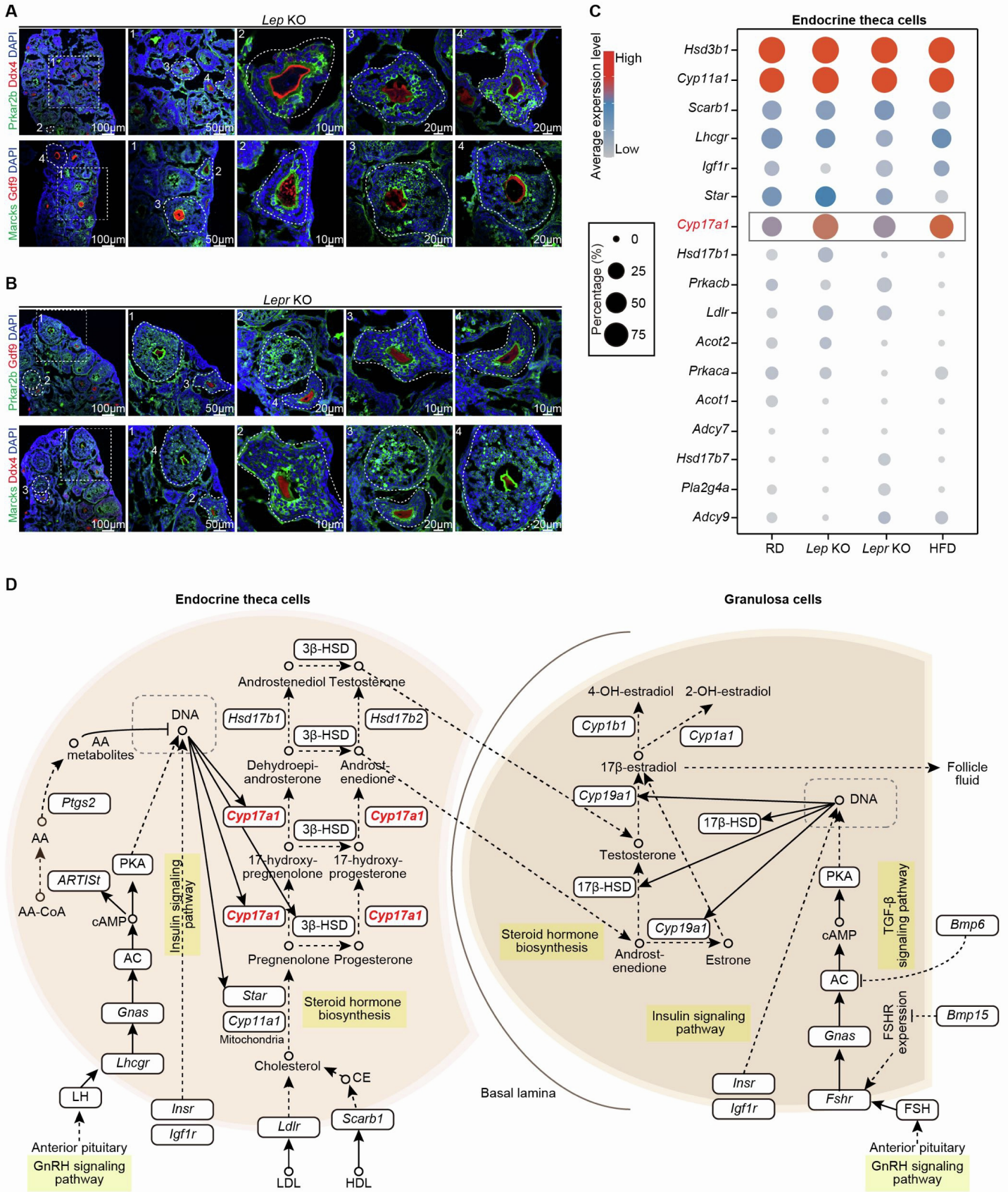


Figure S4. Investigating alterations in ovarian steroidogenesis. Related to Figure 3

A-B, Immunofluorescence staining for Prkar2b and Marcks in ovarian tissues from *Lep* KO (A) and *Lepr* KO (B) mice. Tissues were counterstained with DAPI and Gdf9 or Ddx4.

C, Dot plot showing average expression levels of ovarian steroidogenesis-related genes in ETCs from RD mice and obese mice. Average expression levels were derived from natural logarithm-scaled normalized counts based on single-cell RNA-seq data. The percentage of cells expressing the respective gene is represented by the size of the dot, and only cells with an expression level of greater than 1 for the indicated gene were counted.

D, Schematic overview of ovarian steroidogenesis in *Mus musculus* modified from the KEGG pathway database. Signaling pathways involved are highlighted (yellow). Cyp17a1 is colored in the process of converting pregnenolone to androstenedione and testosterone (red).

Figure S5

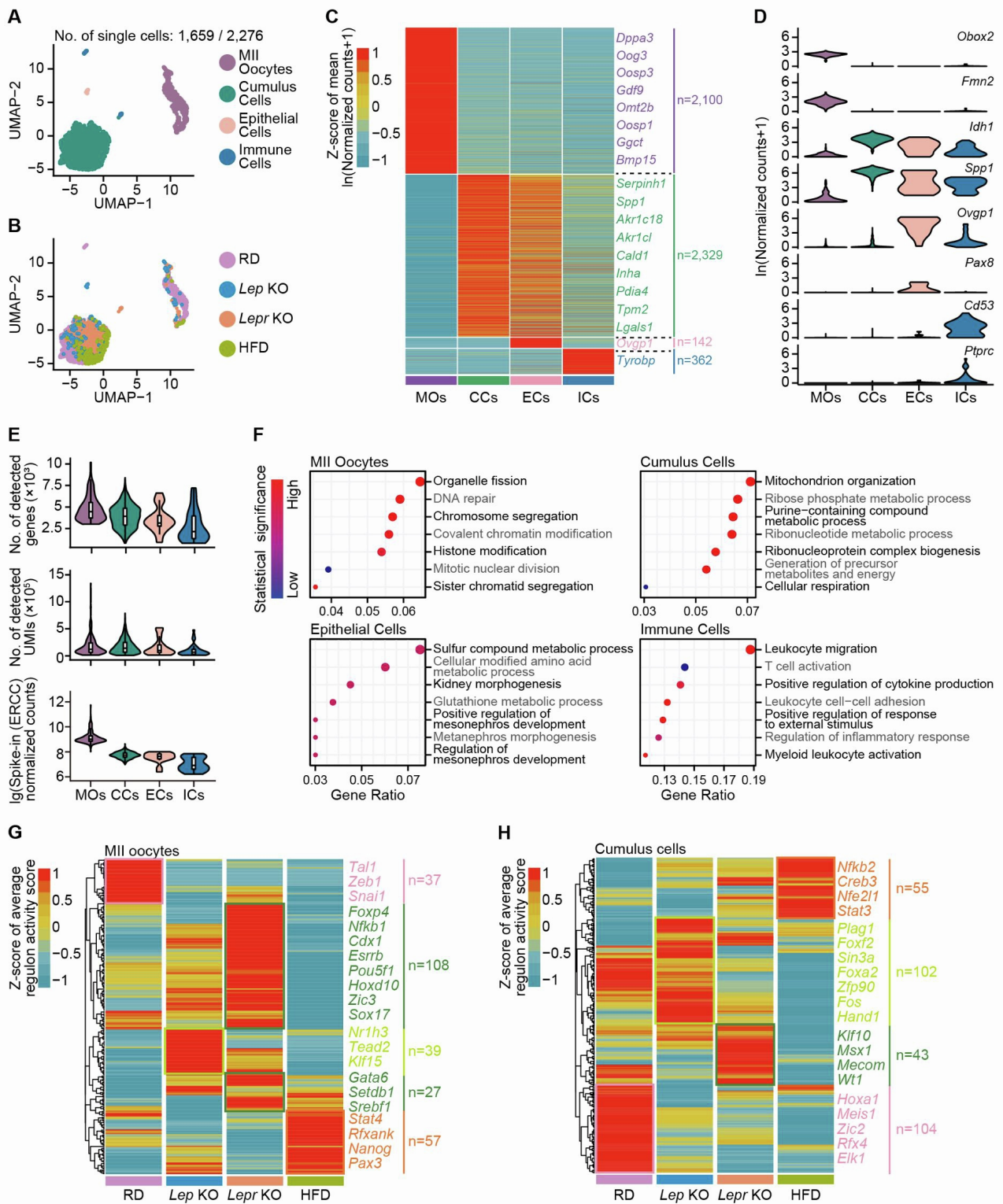


Figure S5. Single-cell gene expression of MII oocytes and cumulus cells from RD and obese mice. Related to Figure 5

A, UMAP embedding visualization of 1,659 single cells from mouse ovulatory follicles showing four major cell populations, including MII oocytes (*Obox2*⁺, *Fmn2*⁺), cumulus cells (*Idh1*⁺, *Spp1*⁺), epithelial cells (*Ovgpl*⁺) and immune cells (*Cd53*⁺, *Ptprc*⁺). Cells are color coded by cell populations.

B, UMAP embedding visualization of cells in (A). Cells are colored by group (RD, *Lep* KO, *Lepr* KO and HFD mice).

C, Heat map depicting differentially expressed genes (DEGs) among all identified cell populations. Gene expression levels were averaged and scaled.

D, Violin plots showing expression levels of representative genes that were explicitly expressed in the indicated cell population.

E, Violin plot of the number of detected genes (top), UMIs (middle), and log-transformed ERCC spikes-in normalized counts (bottom) in an individual cell.

F, Gene Ontology (GO) enrichment analysis for four major cell types identified in (A). These DEGs across all cell populations were investigated for enrichment analysis (overrepresentation test).

G-H, Heat map showing the alterations of transcriptional regulons in MII oocytes (G) and cumulus cells (H) between RD and the obese mice. Regulon activity scores were averaged by group (RD, *Lep* KO, *Lepr* KO and HFD mice) and scaled for visualization.

Figure S6

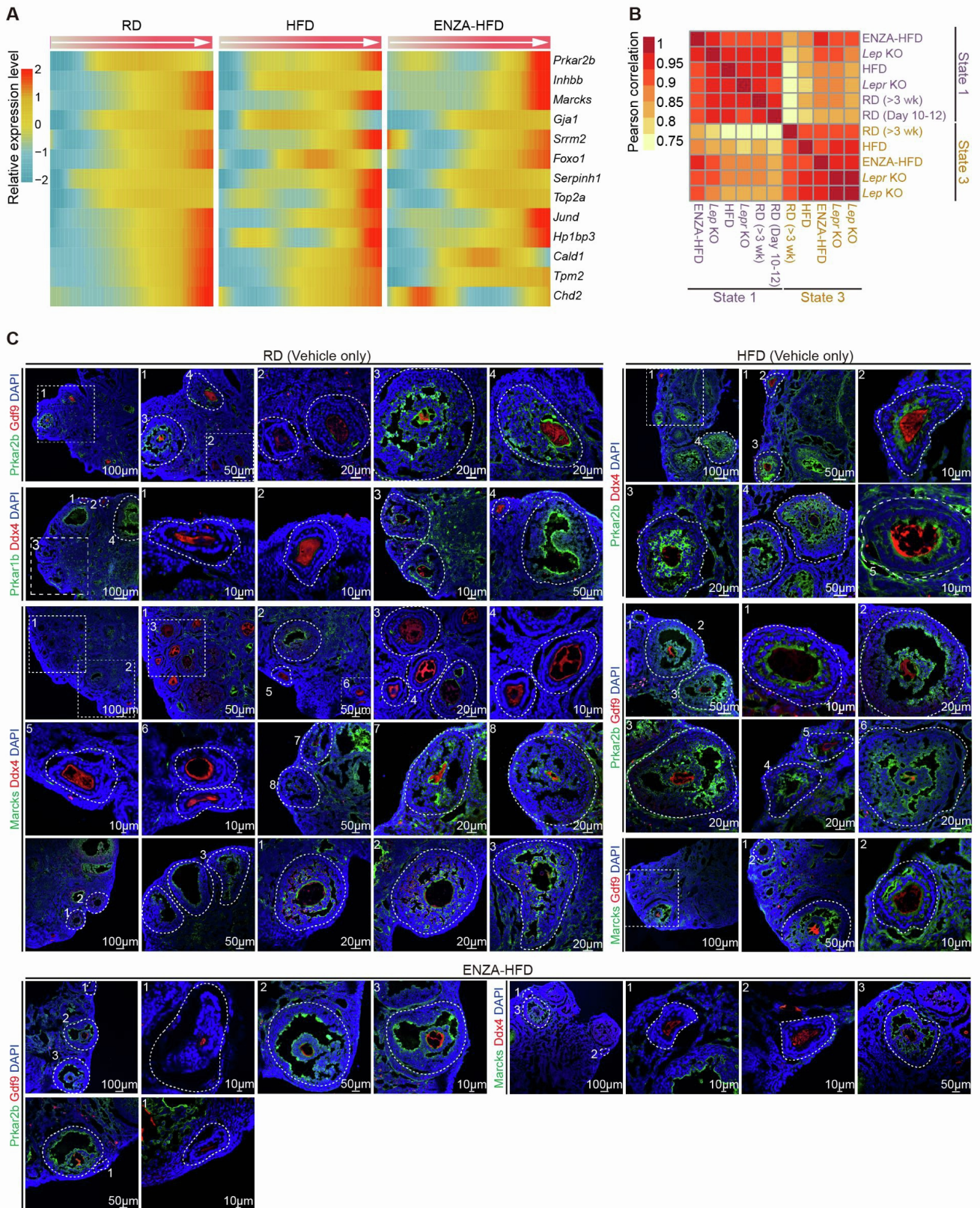


Figure S6. Gene expression in obese GCs after androgen receptor antagonist treatment.

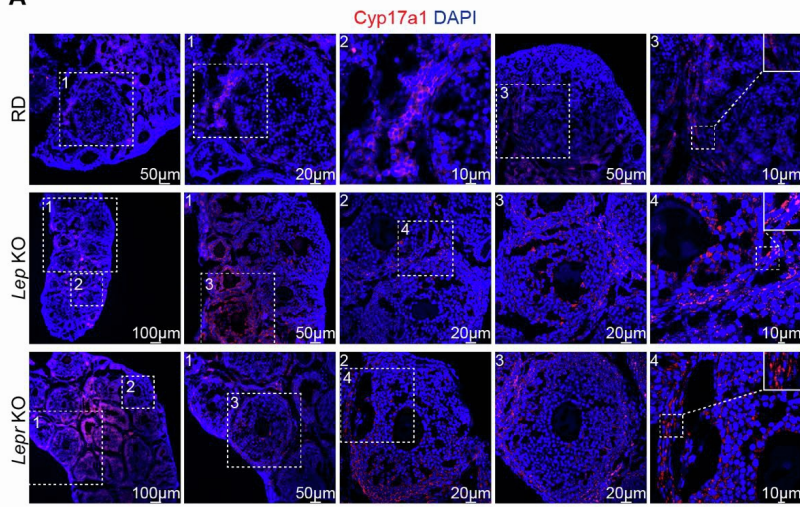
Related to Figure 6

A, Heat map depicting genes with representative pseudotemporal expression patterns in GCs from RD, HFD and ENZA-HFD mice. Gene expression levels were scaled using Monocle2.

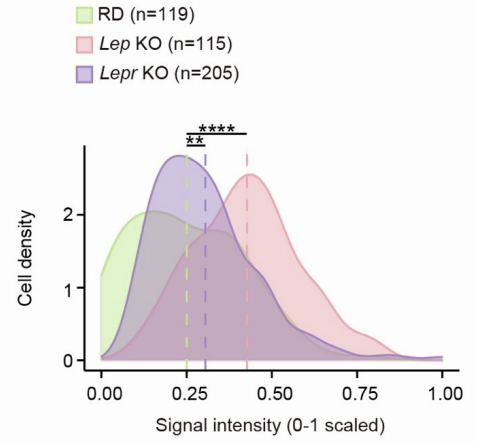
B, Heat map showing the correlation among GCs in different state as indicated. The Pearson correlations were calculated based on the single-cell RNA-seq data.

C, Immunofluorescence staining for Prakar2b and Marcks in ovarian tissues from RD (Vehicle only), HFD (Vehicle only), and ENZA-HFD mice. Tissues were counterstained with DAPI and Ddx4 or Gdf9.

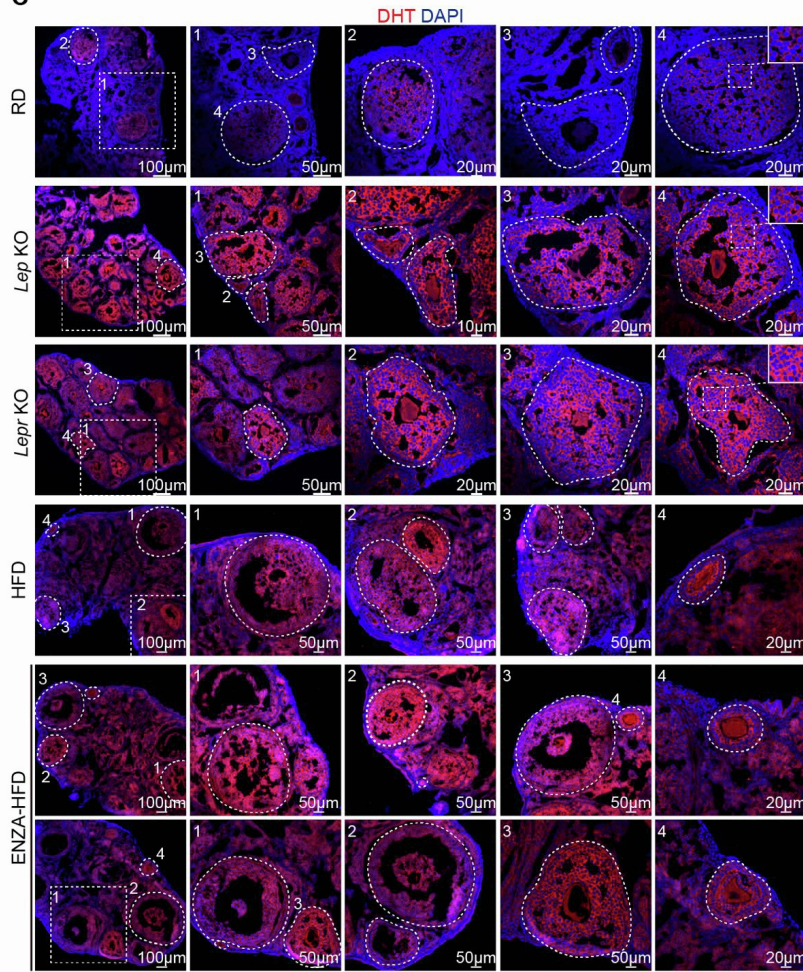
A



B



C



D

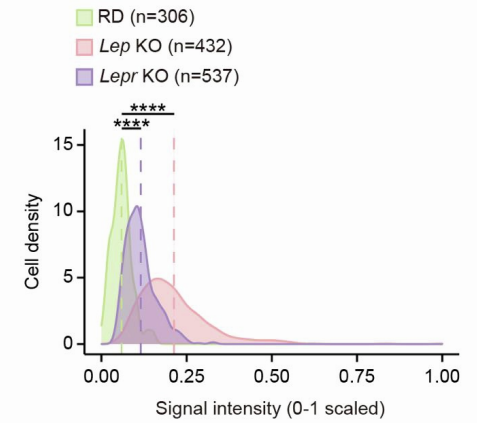


Figure S7. Examination of Cyp17a1 and DHT levels in ovarian tissues from RD, *Lep* KO and *Lepr* KO mice. [Related to Figure 7](#)

A-D, Immunofluorescence staining for Cyp17a1 (A) and DHT (C) in ovarian tissues from RD, *Lep* KO and *Lepr* KO mice. Tissues were counterstained with DAPI. Density plot showing immunofluorescence signal intensity in cells for Cyp17a1 (B) and DHT (D). The signal intensity was measured with Zeiss ZEN. The mean signal intensity of specific antibody staining is indicated as a dashed line. *P \leq 0.05, **P \leq 0.01, ***P \leq 0.001, ****P \leq 0.0001 and n.s. denotes for not significant. (Wilcoxon rank sum test).